STUDY ON 17-4 PH STAINLESS STEEL PRODUCED BY SELECTIVE LASER MELTING

Pierre AUGUSTE[1], Arnold MAUDUIT[1], Lionel FOUQUET[1], Sébastien PILLOT[1]

Specimens of 17-4 PH were manufactured by selective laser melting from two different powders. Depending on the powder used, the specimens' mechanical properties varied, and the microstructures obtained both differed from one another. Observations from electron backscatter diffraction (EBSD) show that, in one case the specimens are mostly ferritic and mostly martensitic in the other.

The mechanical properties and microstructures of these materials following various heat treatments are presented here. In particular, the precipitation caused by ageing treatment of 1 hour – 480°C (H900) hardens both materials, but seems to weaken the material with a ferritic structure. The ferritic specimens that undergo solution heat treatment (1.5 hours – 1040°C) and quenching do not present the mostly martensitic structure expected. To do so, a prior homogenisation treatment is necessary. Finally, a hypothesis is proposed with regards to obtaining the two different structures following an identical manufacturing process.

Keywords: selective laser melting, 17-4 PH stainless steel, martensitic structure, ferritic structure, heat treatment.

1. Introduction

Metal selective laser melting is an additive manufacturing technique, characterised by the layer-by-layer construction of parts: a laser melts the metal powder according to the 3D data entered into a computer. This process is now widely known and described in many documents [1].

Many studies have been undertaken concerning the use of 17-4 PH by selective laser melting. The influence of manufacturing parameters on the material's density, mechanical properties and the microstructure [2] [3] [4] have been researched. The effects of heat treatments and manufacturing direction (layer by layer – generally in Z direction) on the material's mechanical properties [5] have been investigated. Some studies point to the influence of the atomising gas, the protective gas [6] and the nitrogen content [7] on the proportions of residual austenite and martensite present in the manufactured material. Few studies indicate that the structure of 17-4 PH may be mostly ferritic [2] [8] and not interested in it; while it seems very likely that this case is regularly encountered during the production of 17-4PH parts by selective laser melting. Thus obtaining a ferritic structure could explain in some cases inadequate mechanical properties. After characterizing the two powders used, specimens were manufactured from

[1] CETIM Centre Val de Loire (CRAl : Centre de Référence de l'Aluminium, Pole matériaux et procédés) – 9 boulevard Lahitolle, Bourges, France.

them. In the as built temper and after several heat treatments, the microstructures were identified and compared, and the mechanical properties were measured. Finally, a hypothesis is put forward to explain the difference of structure between the two materials following the process.

2. Equipment and methods

Powder-bed laser melting machine

The machine used for this study is a SLM 280 HL from SLM Solutions, equipped with a 400 W YAG laser. Manufacturing parameters are given in Table 1 (standard parameters provided by the machine manufacturer).

Table 1

Manufacturing parameters used.

Layer thickness (µm)	Power (W)	Speed (mm/s)	Hatching (µm)	Base plate temperature (°C)	Base plate material	Protective gas (pure at min 99.99%)
50	275	760	120	200	AISI 310S	Argon

The manufacturing strategy used is known as ‘banding’, with layers crossed at 90° to the others (the first layer with red lines, followed by the second layer with green lines). This is shown in Fig. 1:

- Tracks are produced within adjacent bands, 1 cm wide,
- Bands are oriented identically within the same layer,
- Production is done band-by-band for a single part,
- Tracks are produced in the direction of the band’s width,
- Direction of the tracks’ production alternates,
- The order of manufacturing tracks is shown in Fig. 1,
- The tracks do not follow the direction of the gas flow.

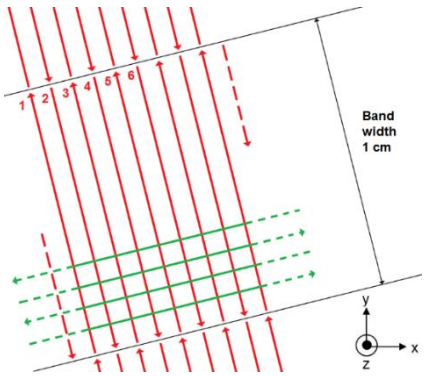

Fig. 1. “Banding” manufacturing strategy – diagram of the slective laser melting process.

17-4 PH – powder – samples

17-4 PH is a precipitation hardening martensitic stainless steel presenting high mechanical properties. This material has high corrosion resistance and good mechanical properties at high temperature. Its chemical composition and its

minimum mechanical properties are specified in the standard ASTM A564/A564M. This material is widely used in aerospace, chemical, petrochemical, agrifood and engineering industries. Its metallurgical structure after casting, solution heat treatment and air cooling is mainly martensitic, with traces of ferrite δ and residual austenite.

Two 17-4 PH powders are used in this study. They are supplied by SLM Solutions and TLS Technik. Their characteristics are given in Table 3 and Fig. 3.

The manufactured specimens are:

- 15 mm-sided cubes (Fig. 2), for metallurgical observations, hardness and porosity measurements,
- 12 mm-diameter, 60 mm-long cylindrical blanks (Fig. 2), for manufacturing tensile specimens.

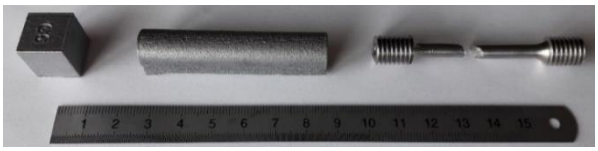

Fig. 2. Cube, cylindrical blank and tensile specimen.

Micrographic examination, SEM and EBSD

Samples for micrographic evaluation were conventionally prepared (cutting, mounting, polishing, micrographic etching, etc.) prior to observation under the optical microscope Zeiss imager M2m AXIO. For informational purposes, a Marble etching was used. Similarly, samples for Scanning Electron Microscopy (SEM) were prepared in the same way as before and observed under a SEM Zeiss EVD, equipped with Energy Dispersive X-ray Spectroscopy (EDS) and EBSD sensors. Determining the phases (distinguishing the ferritic, austenitic and martensitic phases) is one of the attractions of the EBSD technique.

Chemical analysis

The chemical composition of the manufactured material is determined by inductive coupled plasma and atomic emission spectroscopy (ICP-AES). The iron concentration is determined through difference. The device used is an optima 7300 DV. The chemical composition of the powders is identical to that of the manufactured specimens which means that no chemical element has evaporated.

Heat treatments

Heat treatments were performed in a Nabertherm furnace, model N7/H. The fluid used for quenching is ILOQUENCH 52 oil from Castrol. The transfer time in all circumstances is under 7 sec.

Table 2 gives details of the heat treatments applied. A corresponding name, used throughout the rest of this document, is proposed.

Table 2

Heat treatments performed and corresponding name.

Heat treatment following manufacture	Corresponding name
None (**As B**uilt)	AsB
Tempering 1 hr – **480**°C	T480
Tempering 4 hrs – **550** °C	T550
Tempering 4 hrs – **620** °C	T620
Tempering 2 hrs – **760**°C then 4 hrs – 620°C	T760
Solution **H**eat **T**reatment 1.5 hrs – 1040°C + quenching + **T**empering 1 hr – **480**°C	SHT-T480
Homogenisation 2 hrs – 1190°C + **S**olution **H**eat **T**reatment 1.5 hrs – 1040°C + quenching + **T**empering 1 hr – **480**°C	H-SHT-T480

Hardness tests

Vickers hardness (HV30) measurements were performed at room temperature with an Emco Duramin 500 test machine, in accordance with standard ISO 6507-1 (the dewlling time is 14^{+1}_{-4} secondes). Three measurements were performed per specimen (only the average is given).

Tensile tests

Tensile tests were performed in accordance with standard ISO 6892-1 with a Zwick Z250 tensile machine (250 kN). The test speed is 5 mm/min.

Results and analysis

Preliminary results

Powder

The particle size of the powders is measured using a laser granulometer (model mastersizer 3000 Malvern). The SLM powder has a tighter particle size distribution than the TLS powder (Table 3). Particles of both powders are generally spherical (observation by SEM).

Table 3

Particle morphology and size of powders used.

Supplier	Powder characteristics			
	D_{10} (µm)	D_{50} (µm)	D_{90} (µm)	Morphology
TLS Technik	9.3	27.3	57.3	Spherical
SLM Solutions	20.4	32.5	50.1	Spherical

With D_{xx} is the diameter for which xx% of the number of particles are smaller.

Specimens

Table 4 gives the chemical composition of the SLM and TLS samples as built. The TLS material doesn't comply with the standard ASTM A564/A564M. The TLS material has a niobium content three times higher than that of the SLM material. SLM has clearly higher levels of carbon and nitrogen.

Table 4

Chemical composition of the manufactured specimens.

	C%	Mn%	P%	S%	Si%	Cr%	Ni%	Cu%	Nb%	Ta %	N%	Fe %
SLM	0.037	0.63	0.023	0.005	0.69	16.6	4.3	3.9	0.20±0.02	-	0.085	Bal
TLS	0.021	0.57	0.011	< 0.005	0.68	15.8	4.0	3.5	0.60±0.07	-	0.059	Bal
ASTM Limits	0.07	1.00	0.040	0.030	1.00	15.00-17.00	3.00-5.00	3.00-5.00	Nb% + Ta% 0.15-0.45		NS	Bal

The porosity measurements performed on all the cubes show porosity levels systematically below 1%, on average 0.40%, by the Archimedes method [9].

The results of the hardness measurements and tensile tests are given in Fig. 3, 4 and 5. The minimum values corresponding to the H900 temper (ageing treatment : 1 hour – 480°C) of the standard ASTM A564/A564M are given for comparison. When the term SLM is indicated in the designation, it means that the heat treatments have been applied to samples produced with the SLM powder. When there is no indication SLM, it means that the treatments are performed on specimens made with TLS powders.

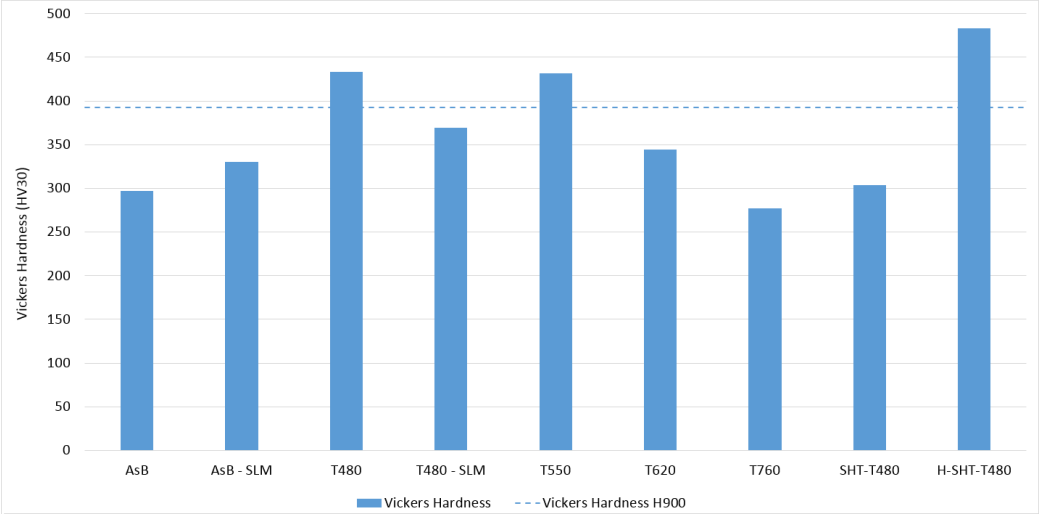

Fig. 3. Hardness measurements in as built temper and after various heat treatments

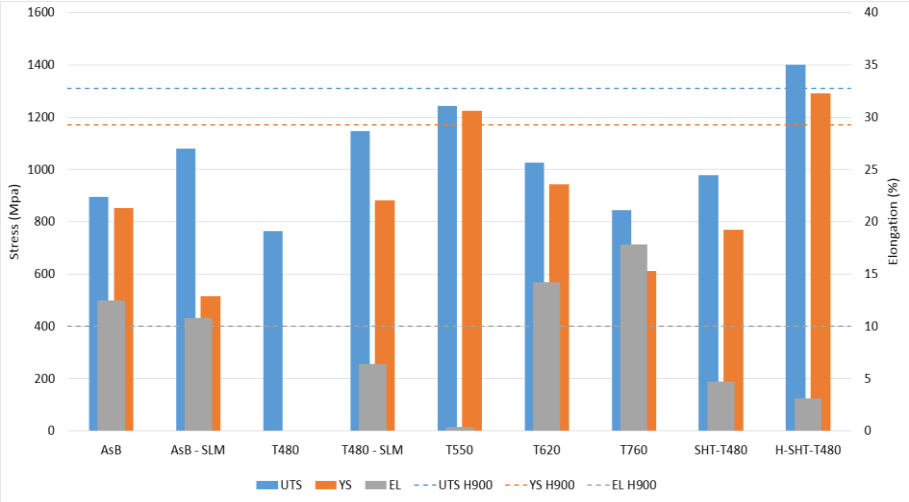

Fig. 4. Tensile tests results of manufactured specimens along the XY axes

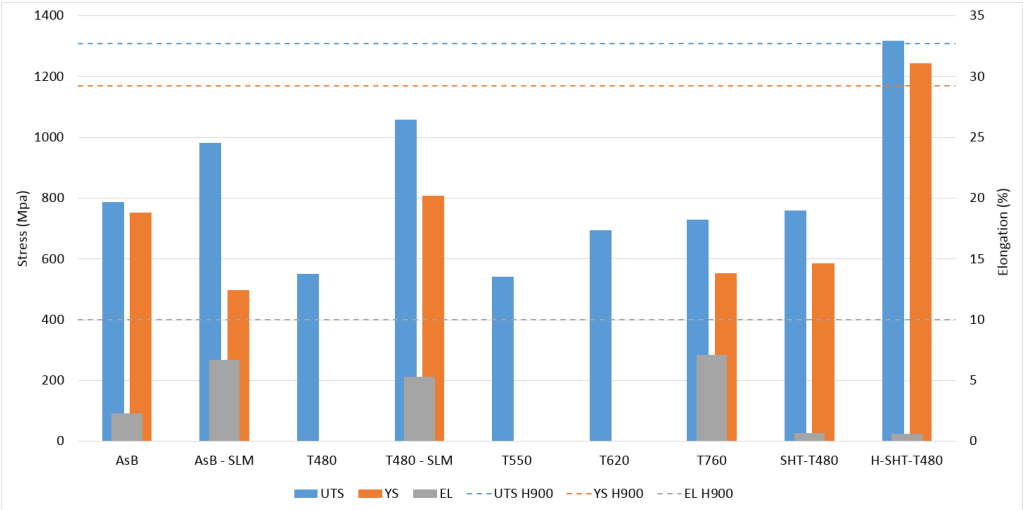

Fig. 5. Tensile tests results of manufactured specimens along the Z axis

3. Results as built

Static mechanical properties

Mechanical properties are given in Fig. 4 and Fig. 5. Mechanical tensile behaviours differ for the TLS and SLM specimens:

- The TLS specimens have lower ultimate tensile strengths (UTS),
- The TLS specimens have higher yield strengths (YS),
- The TLS specimens have smaller elongations at break (EL),
- The mechanical properties for both materials are weaker on the Z axis than on the XY axes. This anisotropy of the mechanical properties is characteristic of the process [5].

These findings suggest that important differences in structure exist between the specimens of the two materials despite the use of an identical manufacturing process.

Observations of the metallurgical structures

Identification of the microstructures of the 17-4 PH as built was difficult. Indeed, the metallurgical structures do not resemble the structures obtained after casting or after welding. In addition, the structures of the SLM and TLS specimens are different. The manufacturing tracks (Fig. 6) are more difficult to identify in the SLM specimens than in the TLS ones. Some tracks of the SLM material can be distinguished in a matrix of small grains.

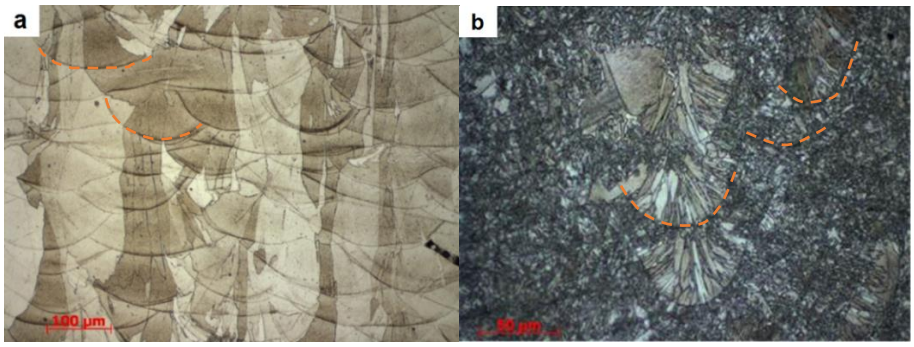

Fig. 6. Observation of the manufacturing tracks (underlined in red) of TLS (a) and SLM (b) materials.

The SLM material is constituted of randomly oriented fine grains, presenting sizes from around 1 to 20 µm at longest (Fig. 7b). The TLS material is composed of :

- Most zones have large elongated grains with a relatively large size of some tens of micrometres to several hundreds. These grains cross several manufacturing tracks and are generally oriented along the Z axis (Fig. 7c).
- Other minor zones present small irregularly shaped grains (Fig 7c – highlighted in blue), with a size of a few micrometres, and without preferential orientation (Fig. 7d - example of areas highlighted in blue). The morphology of these grains is very close to that of the SLM samples.

These two grain structures are different from that usually observed on wrought 17-4 PH (Fig. 7a). In the latter, the grains are discernible by their boundaries in a darker shade of grey, potentially interspersed with white areas of ferrite δ, and are visibly comprised of martensite laths.

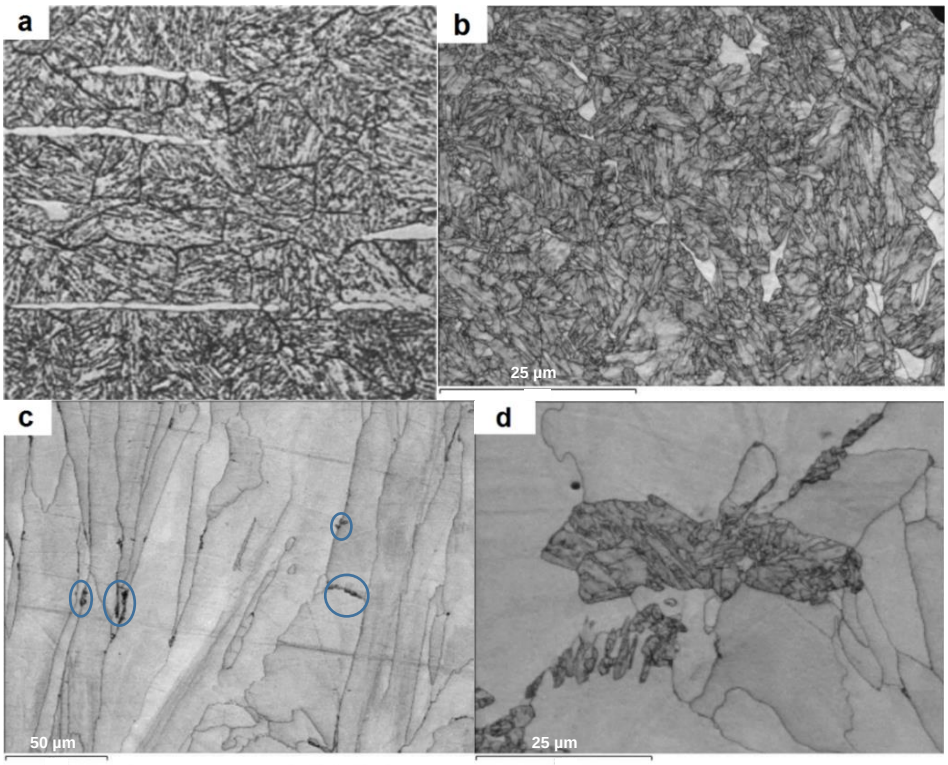

Fig. 7. SEM observation of the grains of the wrought samples (a), SLM (b) and TLS (c, d).

Given the rapid cooling conditions during the process, one expects to find the SLM and TLS samples mainly martensitic, but this phase structure is not recognizable on the photos taken. The EBSD analyses were then performed to determine the microstructures of the samples not easily identifiable by optical microscopy, based on the photos of Fig. 7.

The EBSD analyses highlight the mainly martensitic structure of the SLM sample (Fig. 8a corresponding to Fig. 7b), with the occasional presence of small grains of ferrite and residual austenite. The large grains observed in the TLS sample are ferritic (Fig. 8b corresponding to Fig. 7c), and the minor zones with small grains have a martensitic structure with traces of ferrite and residual austenite (Fig. 8c corresponding to Fig 7d). These differences in structures explain the mechanical properties obtained. The martensite formed in the SLM samples has a little carbon content, which explains its relatively low level of hardness and good ductility. However, the ferrite formed in the TLS samples has abnormally high hardness and relatively low ductility. Given that the SLM and TLS powders were processed with identical manufacturing parameters, it is clear that the process is not alone responsible for this difference in structure.

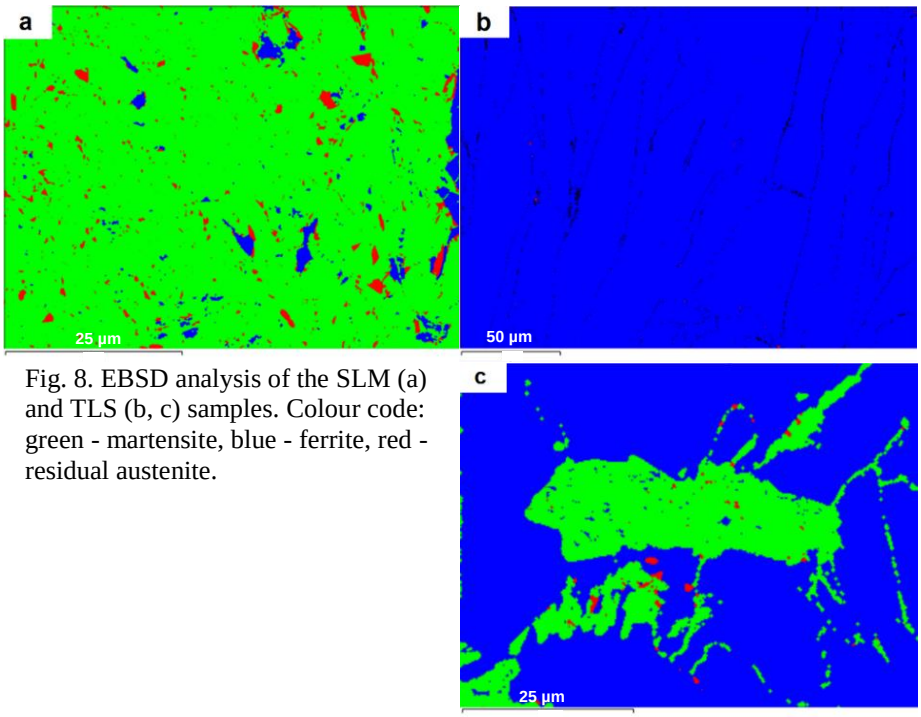

Fig. 8. EBSD analysis of the SLM (a) and TLS (b, c) samples. Colour code: green - martensite, blue - ferrite, red - residual austenite.

Matching SEM observations and EBSD analyzes enables visual identification of the metallurgical structures composing the samples. Thus, Fig 6a is identified as a ferritic structure and the structures of Fig 9a-b also. Then, the phases of the samples having undergone heat treatments are determined by optical microscopy later in this paper.

4. Results after heat treatments

Mechanical properties

The T480 treatment leads to precipitation hardening, which can be detected by the increased hardness (Fig. 3), although this has the effect of making the TLS material brittle. The minimum mechanical properties specified for the H900 temper are not achieved for the two materials. For the TLS samples, the various heat treatments performed offer a compromise between the values of UTS, YS and EL. However, these remain below the minimums of the standard ASTM A564/A564M. The specimens produced along the Z axis have weaker mechanical properties and increased brittleness for the T550 and T620 tempers (Fig. 5).

The mechanical properties obtained for the TLS material in the SHT-T480 temper barely achieve those of the AsB temper, for the XY and Z manufacturing axes. This result suggests that the TLS material does not react to solution heat treatment. The H-SHT-T480 treatment allows the TLS specimens to exceed the values of UTS and YS of the H900 treatment.

Observation of microstructures

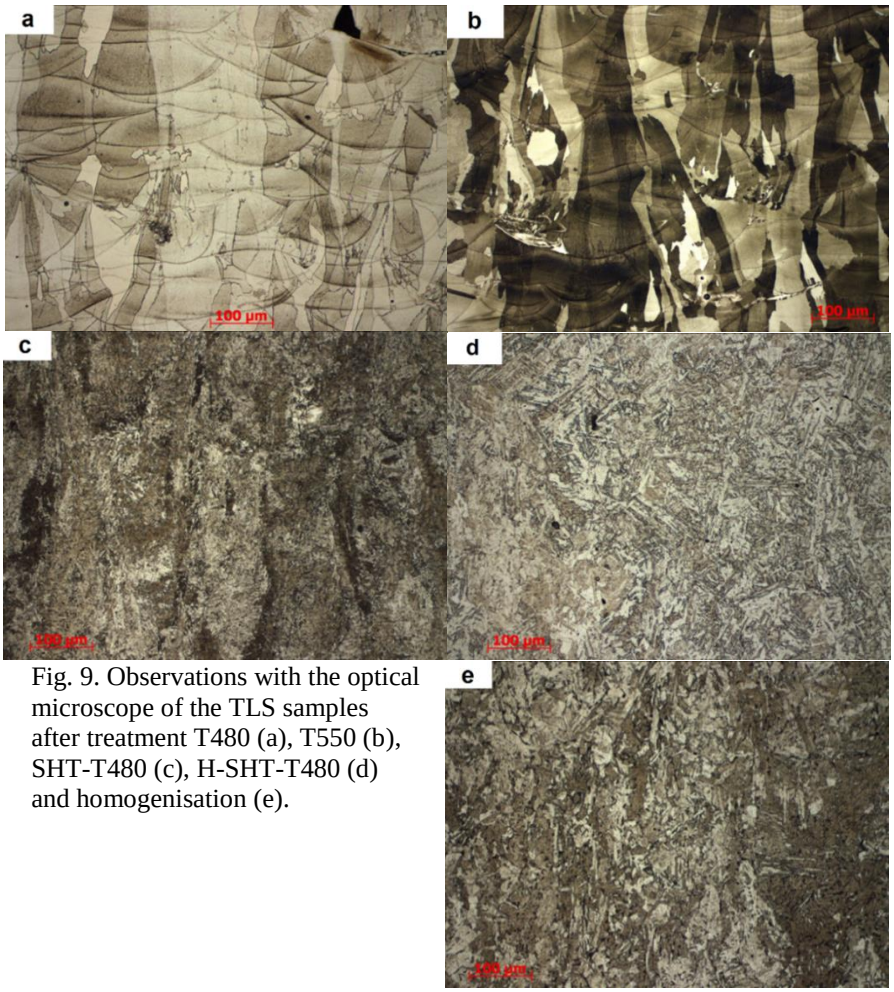

Fig. 9. Observations with the optical microscope of the TLS samples after treatment T480 (a), T550 (b), SHT-T480 (c), H-SHT-T480 (d) and homogenisation (e).

There is no evolution of the microstructure with the tempering (Fig. 9a, b), which confirms that evolution of the mechanical properties is related to precipitation (not observable in optical microscopy).

The structure obtained after SHT-T480 (Fig. 9c) is not defined as martensitic and does not have its mechanical properties. This observation indicates that the material does not react correctly to the solution heat treatment. The purpose of this treatment is to dissolve the copper-rich precipitates in the solid solution and to form an austenitic structure, suitable for obtaining martensite following quenching from this temper. As the final martensitic structure is not observed, it is probable that the desired austenitic structure following solution heat treatment had not been obtained.

The H-SHT-T480 treatment gives rise to a martensitic structure (Fig. 9d), with the expected mechanical properties. As the homogenisation temperature is higher than the solution heat treatment temperature, conversion of the ferrite into austenite is complete and quenching achieves a martensitic structure comparable to that of the wrought 17-4 PH (Fig. 7a).

The structure obtained after homogenisation followed by air cooling (Fig. 9e) is difficult to recognise, but it resembles a martensitic structure.

5. Discussion

To explain the difference in structure between the SLM and TLS parts, it is necessary to understand the behaviour of these materials, from the liquid state to ambient temperature. Firstly, it is important to know the solidification structure (austenite, ferrite or a mixture of the two). Account has to be taken of the rapid cooling and the heating/cooling cycles during the production of the adjacent and upper tracks, while considering any changes of phase likely to occur. Furthermore, the chemical composition is decisive, as it affects the previous parameters.

When a slow cooling speed is applied to the 17-4 PH in liquid state, it is possible to predict its solidification structure from its chemical composition, thanks to formulas for calculating the percentages of equivalent chromium and equivalent nickel [10] :

$$(Cr)_{eq} = (\%Cr) + (\%Mo) + 0{,}7(\%Nb) \quad (1)$$

$$(Ni)_{eq} = (\%Ni) + 35(\%C) + 20(\%N) + 0{,}25(\%Cu) \quad (2)$$

When the ratio $(Cr)_{eq}/(Ni)_{eq}$ is greater than the critical value 1.5, which is the case for the two materials (Table 5), solidification mainly occurs in the form of ferrite δ. Nevertheless, for rapid cooling speeds, this critical value increases and prediction of the solidification structure is not as simple. The solidification structure may then b e austenitic when the cooling speed increases [11] :

Table 5

Values of equivalent chromium and equivalent nickel and related ratio.

Sample	(Cr)eq	(Ni)eq	Ratio (Cr)eq/(Ni)eq
SLM	16.87	8.27	2.04
TLS	16.33	6.79	2.41

In the case of a 17-4 PH solidified in the ferritic phase and cooled at slow speed, conversion of the ferrite into austenite takes place when it goes through the austenitic domain. This allotropic conversion is controlled by a diffusion mechanism of solute atoms, which means it depends on the cooling speed. In

welding, the cooling speed is relatively high, here greater than 10^2°C/s. Conversion of the ferrite into austenite is not complete and the material contains residual ferrite [12]. In the case of selective laser melting, the cooling speed is around 10^5°C/s [13] and one can expect a delay or complete suppression of this conversion, which would have the effect of conserving a ferritic structure. If it is considered that the TLS material is solidified in a mostly ferritic structure, which is probable given the calculated ratio $(Cr)_{eq}/(Ni)_{eq}$, the previous reasoning provides an explanation for obtaining the ferritic structure.

Regarding the SLM material, the calculated ratio $(Cr)_{eq}/(Ni)_{eq}$ is lower than that of the TLS material, even if it is greater than the critical value 1.5. As explained above, the material's high cooling speed causes an increase of this critical value, potentially greater than that of the SLM material and less than that of the TLS material. Thus, the solidification structure of the SLM material would be mainly austenitic. The material's rapid cooling would then have the effect of setting the austenitic structure, preventing its conversion into ferrite α. The conversion of austenite into martensite would happen at the end of manufacture, during the return to ambient temperature, because the temperatures of martensite start and martensite end are around 132°C and 32°C respectively [12]. The final structure of the SLM material would then be mostly martensitic, with traces of residual austenite and ferrite, in accordance with the observations made.

However, solidification of the SLM material into a mostly austenitic phase from the liquid state is not evident. Indeed, while rapid cooling causes an increase of the critical value of the ratio $(Cr)_{eq}/(Ni)_{eq}$, it is possible that this remains less than the value of the SLM material's ratio, and solidification would then occur mostly in the form of ferrite δ. In this case, obtaining a martensitic structure following manufacture means that the ferrite is converted into austenite during the cooling. At first sight, this hypothesis seems to contradict obtaining the ferritic structure of the TLS material. Indeed, the manufacturing parameters, and thus the cooling speeds used, are identical, yet conversion of the ferrite δ into austenite did not occur for the TLS material. This hypothesis can be explained by the difference in chemical composition between the two materials. The SLM material has higher carbon, nitrogen, nickel, copper, and chromium content, and lower niobium content than the TLS material (Table 4). Carbon and nitrogen are two strongly gamagenic elements that are present in a greater proportion in the SLM material. Nickel and copper are also gamagenic. These elements are less soluble in ferrite than in austenite, which favours the latter's conversion kinetics and stability. Niobium is alphagenic and its presence in the TLS material is greater by a factor of three. Also, its content is relatively significant compared to carbon and nitrogen, which favours the formation of niobium carbo-nitrides and limits the formation of austenite [13]. These prevent precipitation of chromium carbides that are embrittling and harmful for the material's corrosion resistance, but they

deplete the matrix of carbon and nitrogen, favouring the ferrite's stability. These elements bring about greater stability of the ferrite for the TLS material than for the SLM material.

With reference to the Fe-Cr-Ni diagram (Fig. 10), the contents of chromium and nickel reveal that the two materials are located at the edge of the austenitic domain. The higher content of gamagenic elements for the SLM material generates an expansion of the austenitic domain and thus a favoured conversion into austenite. In contrast, the higher content of alphagenic elements in the TLS material means a brief passing through or no passing through in the austenitic domain, and thus the formation of a low amount of austenite. In this way, despite rapid cooling, in the case of the SLM material, the passing through the austenitic domain would be sufficient to convert almost all the ferrite into austenite. The final structure of the material would then be mostly martensitic, in accordance with the observations.

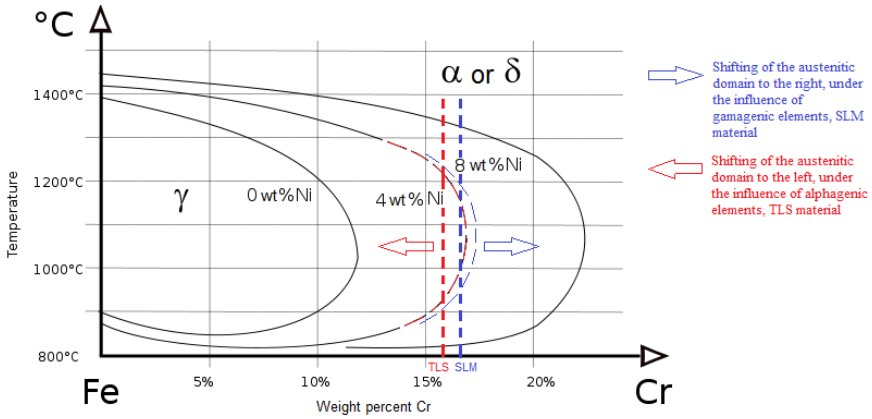

Fig. 10. Cross-section of the Fe-Cr-Ni ternary phase diagram showing the evolution of the austenitic domain according to nickel content [14].

6. Conclusion

This study proposes a comparison of two 17-4 PH manufactured by selective laser melting, from powders coming from two suppliers. The mechanical properties and metallurgical structures were studied for several tempers, and this research leads to the following conclusions:

- In the as built temper, the TLS material is mostly ferritic, and the SLM material is mostly martensitic. This difference is found again in the mechanical properties of the specimens.
- The appearance of the metallurgical structures is conditioned by the high cooling speed and the chemical composition of the materials.
- The TLS material solidifies into a ferritic structure, which is found again at ambient temperature.

- Two hypotheses for obtaining the structure of the SLM material are put forward. If the solidification is ferritic, conversion into austenite takes place. If the solidification is austenitic, this structure is retained during cooling. In both cases, austenite leads to a martensitic structure during cooling.
- Finally, the treatment H-SHT-T480 achieves a martensitic structure for the TLS material.

Acknowledgements

The authors thank all the partners of the SUPCHAD (Supply Chain for Aeronautics and Defense) programme – Cetim, Safran Electronics & Defense, Zodiac Aerospace, MBDA, ThyssenKrupp, Roxel, Mkair and Mecabess – for the funds and help provided in carrying out this study.

R E F E R E N C E S

[1]. *S. Pillot*, Fusion laser sélective de lit de poudres métalliques. Techniques de l'ingénieur BM7900, 2016.
[2]. *A. Kudzal, B. McWilliams, C. Hofmeister, F. Kellogg, J. Yu, J. Taggart-Scarff, J. Liang*, Effect of scan pattern on the microstructure and mechanical properties of Powder Bed Fusion additive manufactured 17-4 stainless steel. Materials and Design, **vol. 133**, 2017, pp. 205-215.
[3]. *H. Gu, H. Gong, D. Pal, K. Rafi, T. Starr, B. Stucker*, Influences of Energy Density on Porosity and Microstructure of Selective Laser Melted 17-4 PH Stainless Steel, University of Louisville, 2013.
[4]. *Z. Hu, H. Zhu, H. Zhang, X. Zeng*, Experimental investigation on selective laser melting of 17-4PH Stainless Steel. Optics & Laser Technology, **vol. 87**, 2016, pp. 17-25.
[5]. *A. Yadollahi, N. Shamsaei, S. M. Thompson, A. Elwany, L. Bian*, Effects of building orientation and heat treatment on fatigue behavior of selective laser melted 17-4 PH stainless steel. International Journal of Fatigue, **vol. 94**, no. 12, 2016, pp. 218-235.
[6]. *L. E. Murr, E. Martinez, J. Hernandez, S. Collins, K. N. Amato, S. M. Gaytan, P. W. Shindo*, Microstructures and Properties of 17-4 PH Stainless Steel Fabricated by Selective Laser Melting. Journal of Materials Research and Technology, **vol. 1**, no. 3, 2012, pp. 167-177.
[7]. *T. L. Starr, K. Rafi, B. Stucker, C. M. Scherzer*, Controlling Phase Composition In Selective Laser Melted Stainless Steel, University of Louisville, 2012, pp. 439-446.
[8]. *M. Alnajjar, F. Christien, C. Bosch, K. Wolski*, Caractérisation microstructurale de l'acier inoxydable 17-4PH obtenu par fabrication additive SLM. Journées annuelles SF2M 2017, Saint-Etienne.
[9]. A. Mauduit, S. Pillot, F. Frascati, Application study of AlSi10Mg alloy by selective laser melting: physical and mechanical properties, microstructure, heat treatments and manufacturing of aluminium metallic matrix composite (MMC). Metallurgical research and technology, n°112, 605, 2015.
[10]. *W. Liu, J. Ma, M. Atabaki, R. Pillai, B. Kumar, U. Vasudevan, H. Sreshta, R. Kovacevic*, Hybrid laser-arc welding of 17-4 PH martensitic stainless steel. Lasers in Manufacturing and Material Processing, Research Center for Advanced Manufacturing, Dallas, 2015.
[11]. *S. A. David, J. M. Vitek, R. W. Reed, T. L. Hebble*, Effect of rapid solidification of stainless steel weld metal microstructures and its implications on the schaeffler diagram. Oak Ridge National Laboratory, 1987.
[12]. *H. K. Rafi, D. Pal, N. Patil, T. L. Starr, B. E. Stucker*, Microstructure and Mechanical Behavior of 17-4 Precipitation Hardenable Steel Processed by Selective Laser Melting. Journal of Materials Engineering and Performance, **vol. 23**, no. 12, 2014, pp. 4421-4428.
[13]. *M. Averyanova*, Fusion laser de poudres métalliques: Maîtrise du procédé pour la fabrication directe de pièces mécaniques. PhD Thesis, ENISE Saint-Etienne, 2011.
[14]. *P.J. Cunat*, Aciers inoxydables – Critères de choix et structure. Techniques de l'ingénieur, M4540 v1, 2000.